The Complex Image Method for Simulating Wave Scattering in Room Acoustics

1st Orchisama Das
Institute of Sound Recording
University of Surrey
Guildford, United Kingdom,
o.das@surrey.ac.uk

2nd Enzo De Sena
Institute of Sound Recording
University of Surrey
Guildford, United Kingdom,
e.desena@surrey.ac.uk

***Abstract*—The Image Method (IM) has become increasingly popular for small-room acoustics simulations. While it gives an exact solution of the wave equation in shoebox-rooms with rigid walls, the assumption of rigidity is not valid in real rooms. Based on spherical wave reflection from an infinite wall, several authors have independently developed what is known as the Complex Image Method (CIM). However, its adoption in room acoustics has been rare, although it has been shown to give performance equivalent to the boundary element method in shoebox rooms with soft-walls. In this paper, we review the theory behind CIM and provide a Python implementation to study directional scattering patterns as a function of wall impedance. For a highly symmetrical room, room impulse responses simulated with CIM are shown to have less so-called "sweeping echoes" than those simulated by IM.**

***Index Terms*—room acoustics, image method, scattering**

I. Introduction

Geometrical acoustics has become widely popular for rendering reverberation in architectural acoustics and XR (extended reality) applications [1]. While the methods are mature, efficient and provide high perceptual accuracy in the high-frequency regime, all wave phenomena associated with longer-wavelength sound waves are ignored — such as scattering and diffraction. Many work-arounds have been suggested in the geometrical acoustics community to handle these phenomena [2], [3], but these are often an approximate solution to the physics. On the other hand, there are highly accurate wave-based methods, such as Finite-Difference Time-Domain (FDTD) [4] and Boundary Element Method (BEM) [5], that are computationally expensive and orders of magnitude more processing time on parallel clusters of processors, making them impractical for many applications.

One particularly popular method in geometrical acoustics is the image-source model [6]. In fact, this method gives an exact solution of the wave-equation in shoebox rooms with rigid walls. Its widely available efficient implementation [7] has made it a favorite of the machine-learning community for artificially generating room impulse responses for large datasets. However, not only is the assumption of rigid wall impractical in real rooms, the method often introduces sweeping echoes in the generated room impulse response due to time-alignment of several symmetric image sources [8]. Since such strong sweeping echoes are not observed in most rooms, De Sena et. al proposed adding a small random displacement in the position of the image sources to break this alignment. It is to be noted that sweeping echoes are observed in all rectangular rooms in varying degrees (as confirmed in [8] with FDTD simulations); however, the phenomenon is greatly exaggerated by the image-method.

In [9], [10], Ingard and Rudnick studied the fundamental problem of spherical wave reflection from an infinite plane with finite impedance. In fact, there was some interest in the acoustics community in developing that theory further into what is known as the *Complex Image Method* [11], [12]. Unlike the image method, the complex image method does not assume rigid walls. In the image method, the wave incident on the rigid wall is reflected back with some frequency-dependent losses, but no scattering is included. The plane wave reflection coefficient is used in IM, but CIM incorporates the spherical wave reflection coefficient. The spherical wave reflection coefficient makes use of the plane wave reflection coefficient, but adds a boundary loss factor due to the spherical wave front. The benefits of using a spherical wave reflection coefficient instead of the plane wave reflection coefficient in room acoustics simulations was investigated by Lam [13].

Lam observed that in a rectangular room the mirrored surfaces form an infinite plane in each of the coordinate planes, which means that the effective reflecting surfaces are all plane with uniform admittance. This situation creates no edge effects and matches well with the configuration assumed by both the plane and spherical wave reflection coefficients. However, the spherical wave reflection model was found to produce predictions in both frequency and time domains that are virtually identical to those by BEM, showing that the spherical wave reflection formulation in a geometrical acoustics model is a valid and accurate model. The plane wave reflection model was found to have noticeable errors at higher admittance (absorptive) values and at longer delay time (higher order reflections).

Despite such significant results, the adoption of the spherical wave reflection coefficient in the image method has been slow. In this paper, we review the complex image method and pro-

This work was funded by the EPSRC grant EP/V002554/1, "SCalable Room Acoustics Modeling" (SCReAM).

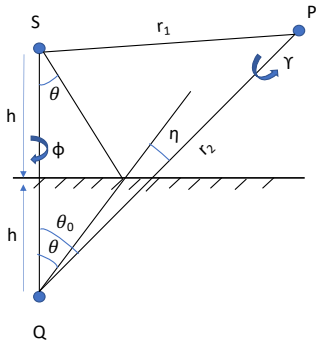

Fig. 1: *Reference geometry*

vide a software implementation[1] that can generate the pressure field at desired frequencies and receiver positions in a shoebox room with soft walls using CIM. This implementation takes in as input room dimensions, source position, microphone array positions, wall impedance and wave numbers to evaluate the solution on, and returns as output the total pressure field at the mic array locations. We use this package to study wave scattering at various frequencies as a function of the wall impedance. It is to be noted that the complexity of CIM is much higher than that of IM as it is implemented in the frequency domain.

The paper is structured as follows. First, we review Ingard's model of spherical wave reflection from an infinite plane in Section II. Then, we detail an algorithm for the image method with spherical wave reflection coefficients in Section III. In our simulations, we study the scattering patterns from a single source above an infinite wall (Section IV-A) and a source placed in a shoebox room (Section IV-B). We observe that the complex-image method considerably reduces sweeping echoes in rectangular room simulations when compared to the image method. We discuss the limitations of our current implementation and propose scope for future work in Section V.

II. Spherical wave reflection from infinite plane

Ingard [9] derived the expression for pressure at the receiver when a spherical wave is reflected from a non-rigid infinite wall. For a point-source emitting a spherical wave, S, at a distance h above an infinite plane, shown in Fig. 1, let the admittance be β. The total pressure at the receiver location, $p_P(k)$, is given by the sum of the incident wave, $p_S(k)$, and reflected wave from the image-source, $p_Q(k)$:

$$\begin{aligned} p_P(k) &= p_S(k) + p_Q(k)\ , \\ p_P(k) &= \frac{\exp\left(jkr_1\right)}{r_1} + p_r(k)\ , \end{aligned} \tag{1}$$

where $k = \omega/c$ is the wave number and r_1 is the distance between the source and receiver location and $p_r(k) = p_Q(k)$ is the reflected wave.

[1]Python implementation available at https://github.com/SCReAM-Surrey/ComplexImageMethod.

Weyl's identity [14] tells us that the spherical wave in the half-plane below the source S, that strikes the non-rigid infinite plane, can be written as a superposition of plane waves,

$$p_S(k) = \frac{\exp\left(jkr_1\right)}{r_1} = \frac{j}{2\pi}\int_{\mathcal{S}} \exp\left(jk[ax+by+c(h-z)]\right)d\omega. \tag{2}$$

in which where k is the wave number, a, b, c are the direction cosines of the propagation vector, x, y, z are the position coordinates, r_1 is the distance from the source to the wall, $d\omega = \sin\theta d\theta d\phi$ is the incremental change in solid angle and the domain of integration is the half-plane below the source.

Similarly, the reflected spherical pressure wave with the boundary conditions can be written as a superposition of plane waves weighted by the plane-wave reflection coefficient:

$$p_r(k) = \frac{j}{2\pi}\int_{\mathcal{S}} \exp\left(jk[ax+by+c(h+z)]R d\omega\right. \tag{3}$$

. Here, R is the plane-wave reflection coefficient,

$$R = \frac{\cos\theta - \beta}{\cos\theta + \beta}. \tag{4}$$

Ingard shows that using the direction QP as the axis of a new coordinate system with the angle variables η and ψ, shown in Fig. 1, the integral for the reflected pressure is,

$$p_r(k) = \frac{j}{2\pi}\int_{\psi=0}^{2\pi}\int_{\eta=0}^{\frac{\pi}{2}+j\infty} \exp\left(-jkr_2\cos\eta\right)R(\psi,\eta)\sin\eta d\eta d\psi. \tag{5}$$

Here r_2 is the distance between the image source and the receiver. Making the substitution $\cos\eta = 1 + jt$, one can write,

$$\begin{aligned} p_r(k) &= \frac{\exp\left(jkr_2\right)}{r_2} kr_2 \int_{t=0}^{\infty} \exp\left(-jkr_2\right)\langle R(t)\rangle dt \\ &= \frac{\exp\left(jkr_2\right)}{r_2}\mathcal{Q}, \end{aligned} \tag{6}$$

where $\mathcal{Q}$ is the the strength of the image-source, and $\langle R(t)\rangle$ is the ensemble average of the plane-wave reflection coefficient:

$$\begin{aligned} \langle R(t)\rangle &= \frac{1}{2\pi}\int_0^{2\pi} R(t,\psi)d\psi, \\ R(t,\psi) &= \frac{\cos\theta - \beta}{\cos\theta + \beta} \\ \cos\theta &= \cos(\theta_0 - \eta)\cos\psi. \\ &= \cos\theta_0\cos\eta + \sin\theta\sin\eta\cos\psi \\ &= \gamma_0(1+jt) + \sqrt{(1-\gamma_0^2)t(t-2j)}\cos\psi \end{aligned} \tag{7}$$

Here, $\gamma_0 = \cos\theta_0$, and θ_0 is the angle between the image-source and receiver. After following a series of calculations detailed in [9], the image-source strength, $\mathcal{Q}$, may be written as

$$\begin{aligned} \mathcal{Q} &= R_0 + (1-R_0)\left[1 + j\sqrt{\pi\rho}\, e^{-\rho}\Phi(-j\sqrt{\rho})\right], \\ R_0 &= \frac{\gamma_0 - \beta}{\gamma_0 + \beta}, \\ \rho &= \frac{jkr_2}{2}\frac{(\gamma_0+\beta)^2}{1+\gamma_0\beta}, \end{aligned} \tag{8}$$

where $\Phi(\cdot)$ is the complementary error function. The reflected field is a function of the distance and angle from the image-source to the receiver, and the wall impedance. The total pressure is given by

$$p_P(k) = \frac{\exp(jkr_1)}{r_1} + \frac{\exp(jkr_2)}{r_2}\mathcal{Q}. \tag{9}$$

Unlike geometrical acoustics, where only a finite number of rays are incident on the reflecting plane, we see that a spherical wavefront is incident on the boundary and must be integrated over all directions, as in (3). This is equivalent to what happens in the boundary-element method where the total pressure at the receiver is a sum of the incident pressure and the scattered field from every point on the boundary. Allen and Berkeley's image-source model assumes a rigid wall and ignores the effect of scattering completely. This makes the computation much easier and faster, since no book-keeping of the reduced image-source strength needs to be done.

III. Spherical wave reflection in a shoebox-room

As mentioned in Section I, the spherical wave reflection coefficient gives results closer to BEM when compared to the plane wave reflection coefficient [13]. This is highlighted especially in the lower frequency region (< 200 Hz) in rooms with soft walls, where wave properties dominate. However, uniform admittance is assumed in CIM. Local fluctuations in wall admittance cannot be modelled by this method. The spherical wave reflection coefficient also cannot model surface roughness which is important in modelling high frequency scattering.

In the case of a source and an infinite-plane, there is only one-image source mirrored along the plane. Consider the case of perpendicular planes, as shown in Fig. 2a. The first-order image source of each wall, Q, acts as a secondary source for the other wall. This produces a second-order image source, Q_s. The two secondary image sources overlap in this case. In the case of two parallel planes, as shown in Fig. 2b, there are an infinite order of image sources formed due to successive reflections (only images up to the second order are shown here). However, the strength of these image sources is inversely proportional to the distance from the plane; therefore, they can be truncated beyond a certain order[2].

Since these walls are finite, the limits of integration of η in (5) should change to account for edge-effects. However, Lam [13] argues that in perfectly rectangular rooms, the walls are mirrored along each axis, essentially forming an infinite plane in each coordinate plane. We experimented with changing the limits of integration of η based on the angle made from the point-source to the wall-edge, which effectively changed (8) to include an incomplete Gamma function that misbehaved for complex values of admittance. Hence, in the rest of this paper we work with Lam's assumption of infinite tessellating planes. Lam showed in his investigations that this assumption gives results identical to the BEM for shoebox rooms. For non-shoebox rooms, further investigation of the edge-effects is required.

For a shoebox room with parallel pairs of walls, each image source of the N th wall will act as a virtual source for the other $N-1$ walls, with its unique strength based on the wall impedance, angle and distance to receiver. For N walls and up to K th order image-sources, the algorithm is given in Alg. 1.

In the pseudo-code, i iterates over reflection orders, n, m iterate over walls and k represents a wave number. The function $F(\cdot)$, given by (8), depends on wall impedance, angle and distance from of the image-source to the receiver. The strength of the source for each wall and each reflection order gets scaled recursively, thus attenuating the strength of the higher-order image sources. The first loop iterates over the reflection orders, the second loop iterates over the walls, the third loop iterates over all the image sources of order i and associated with wall n, and calculates the reflected pressure at the receiver due to each image-source. Finally, the image-sources for the next order are calculated and their strength is attenuated based on the strength of the current image-source.

Algorithm 1 Pseudocode for calculating the scattered pressure at the receiver due to the contribution of N walls and up to K th order image sources.

```
p_r ← 0
image-source ← {}
for i = 1, ··· , K do
  for n = 1, ··· N do
    visited-image ← {}
    if i = 1 then
      S_0 ← original source reflected along plane n.
      θ_{S_0}, r_{S_0} ← angle and distance of S_0 from receiver(s).
      Q_{S_0} ← F(β_n, r_{S_0}, θ_{S_0})
      image-source[i, n] ← S_0
    end if
    for S ← image-source[i, n] do
      if S ∈ visited-image then
        continue
      else
        visited-image ← push(S)
        p_r ← p_r + (exp(jkr_S)/r_S) Q_S
        for m = 1, ··· , N, m ≠ n do
          if S not behind wall m then
            S_m ← Image of S, reflected along plane m.
            θ_{S_m}, r_{S_m}, ←
            angle and distance of S_m from receiver(s).
            Q_{Sm} ← Q_S F(β_m, r_{Sm}, θ_{Sm}).
            image-source[i + 1, m] ← append(S_m)
          end if
        end for
      end if
    end for
  end for
end for
```

[2]While the 1/r attenuation decreases the strength of these sources, their number increases polynomially giving.

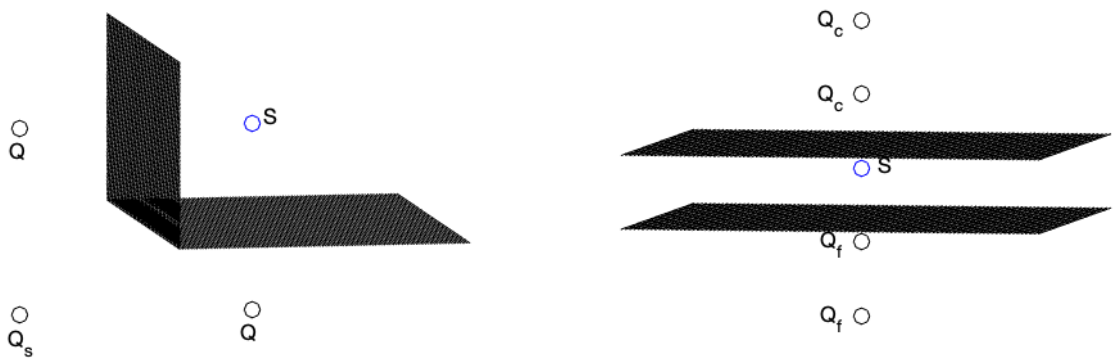

(a) Perpendicular walls

(b) Parallel walls

Fig. 2: Second-order image-sources with source in between two reflecting planes.

To avoid duplication of image-sources, a list of the image sources for each order is maintained.

IV. Evaluation

A. Single wall

In the simplest scenario, we consider an infinite wall in the xy plane. We put an acoustic source at a distance of $kh = 5$ above the plane, where k is the wave number and h is distance from the plane in the z-axis. The pressure field is evaluated at $kr \in [0, 50]$, where k is the wave number and r is the distance from the image source to the receiver. The angle between the image source and the receiver, θ_0, is varied from $-90°$ to $90°$.

The impedance is varied according to $\beta(kr) = \frac{\beta}{1+\exp(-jkr)}$ for $\beta \in [0, 0.1, 1, 10]j$. The reader should note that an admittance of zero corresponds to a rigid wall. The pressure polar patterns for the source above the wall is shown in Fig. 3. The polar angle represents the angle between the image source and the receiver (θ_0). For all impedance values, the distribution is close to being uniform at low values of kr. It becomes highly directional at mid-frequencies when the values of kr and kh are comparable. This represents a scenario when the observer is at the same height as the source. Maximum pressure will occur when they are in line ($0°$). At higher frequencies, the response is also highly directional with off-axis receivers at $45°$ and $90°$ observing maximum pressure. This shows that even in the case of a simple infinite wall with uniform impedance, scattering is highly variable with frequency and wall impedance.

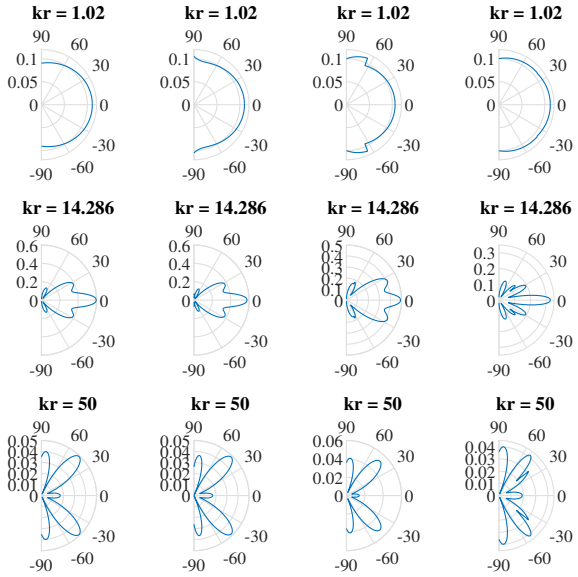

(a) $\beta = 0$ (b) $\beta = 0.09 + 0.15j$ (c) $\beta = 0.89 + 0.55j$ (d) $\beta = 0.80 + 0.03j$

Fig. 3: Polar scattering patterns when a source is placed above an infinite wall at a height of $kh = 5$ with different impedance values. For example, at a frequency of 1 kHz and with $c = 340$ m/s, $k = 18.5$ and $h = 0.27$ m

B. Shoebox room

1) Scattering: To evaluate the pressure field in a room with the complex-image method, a shoebox room of dimensions $4 \times 5 \times 4.5$ m^3 is simulated. The source is placed at $(0.5, 2.3, 1.2)$ m. An array of hundred receivers are placed along an arc on the xz plane from $0°$ to $90°$ at a radius of 2 m. The configuration is shown in Fig. 4a. The pressure field is evaluated for all the receivers at 100 different wave-numbers spanning $50 - 1600$ Hz.

The wall admittance is varied with the frequency as, $\beta = (0.5+0.5j) \times \frac{1}{1+\exp(-\omega/c)}$ $\mho$, where ω is the frequency and c is the speed of sound in air. The complex image method is run up to the fifth order. The results are shown in Fig. 4. The top row of plots show the pressure as a function of the wave number and the angle of receiver for increasing reflection orders from left to right. The bottom row of plots show the polar pattern of the pressure distribution for three specific frequencies, from

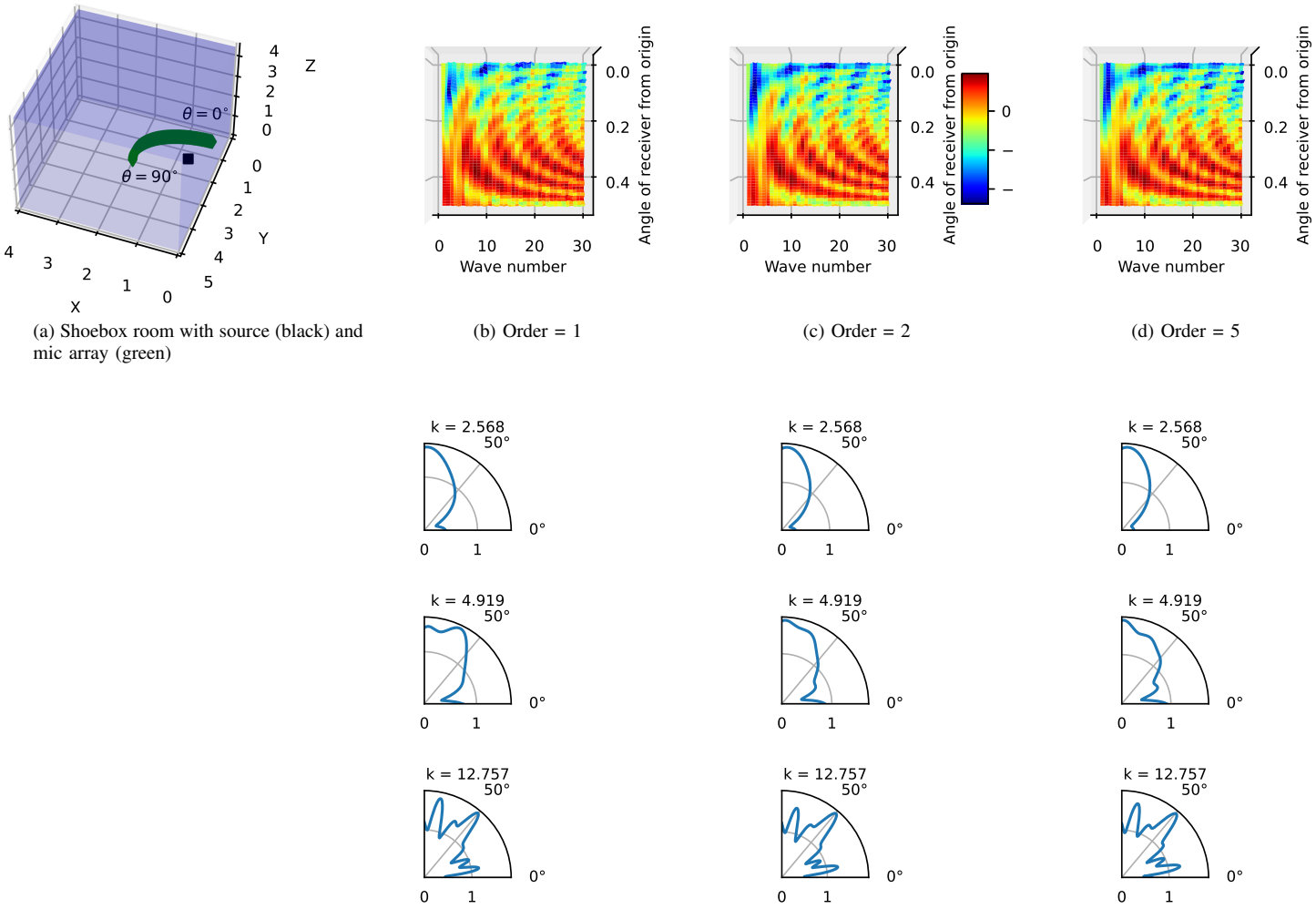

(a) Shoebox room with source (black) and mic array (green)

(b) Order = 1

(c) Order = 2

(d) Order = 5

Fig. 4: Results of the complex image simulation up to fifth order for frequency-dependent admittance on the walls. Top - surface plot, bottom - polar plot showing directional scattering. Reflection orders from left to right - one, two, five.

low to high. At low frequencies ($k = 2.568$ m^{-1}, i.e. $f \approx 117$ Hz for $c = 340$ m/s), a wider main lobe is observed. More complex scattering patterns are observed at higher frequencies, as the number of lobes multiply. The pressure is no longer distributed widely over a region, but in specific directions only.

2) Sweeping echoes: For a shoebox room of $4 \times 4 \times 4$ m^3 , we compared the room impulse response (RIR) generated by the complex image method to that of the image method, as implemented in Pyroomacoustics (PRA). The source was placed at (1,2,2) m and the microphone was placed at (1.5,2,2) m. Air absorption was turned off in PRA. The sampling frequency was 8 kHz and the maximum order of reflections was fixed to be 10. Pyroomacoustics takes as input the absorption coefficient of the room, whereas the complex image method takes the wall admittance as input. The relationship between the absorption coefficient and the wall admittance is given by [15]

$$r = \sqrt{1-a}, \qquad \beta = \frac{1-r}{1+r}. \tag{10}$$

For a rigid wall, ($a = \beta = 0$), the RIRs generated by both methods match exactly in Figs. 5d, 5a, as expected. PRA adds an additional initial delay. The first peak from the direct path should occur at 11.6 ms, as correctly predicted by our implementation. For this configuration, strong sweeping echoes are heard in both the RIRs. These are visible as straight lines intercepting the origin in the associated spectrograms and are caused by time alignment of the image sources of higher orders, as shown by De Sena et al. [8]. The regularity of image sources positions' leads to a monotonic convergence in the time of arrival of the far-field image pairs.

For an absorption coefficient of $a = 0.3 (\beta = 0.089\ \mho)$, the output from the image method (Fig. 5b) has more perceivable sweeping echoes, which would not normally be heard in real rooms due to scattering. Sweeping echoes are reduced (but not eliminated) by the complex image method (Fig. 5e). For an even higher absorption coefficient of $a = 0.5 (\beta = 0.172\ \mho)$, sweeping echoes are nearly eliminated by the complex image method (Fig. 5f). Because the spherical wave reflection

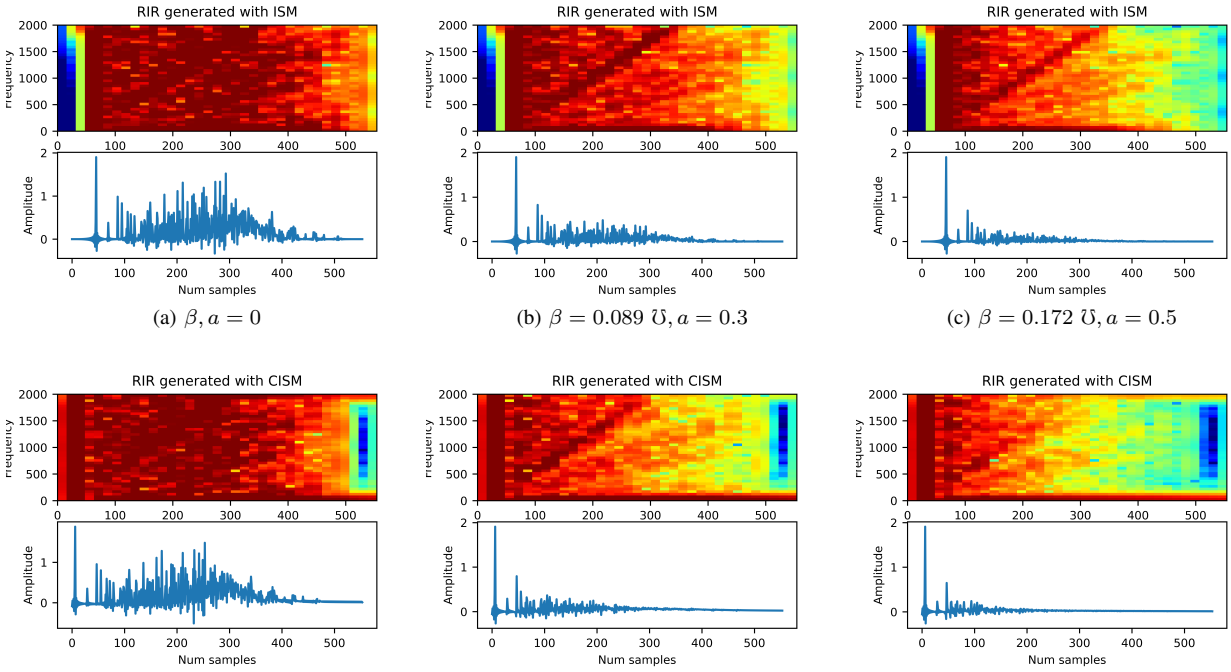

(a) $\beta, a = 0$ (b) $\beta = 0.089\ \mho, a = 0.3$ (c) $\beta = 0.172\ \mho, a = 0.5$

(d) $\beta, a = 0$ (e) $\beta = 0.089\ \mho\mho, a = 0.3$ (f) $\beta = 0.172\ \mho, a = 0.5$

Fig. 5: Comparison of the complex image method (bottom) with the image method (top) for different absorption values.

coefficient is a complex number with non-zero phase, the phase-alignment caused by the contribution from multiple image sources, is broken. Recall that in the image method, the contribution due to each image source is simply scaled by the wall absorption coefficient. Since the complex image method explicitly keeps track of the phase of the reflected wave, it eliminates time-alignment of the image-sources which leads to sweeping echoes in highly symmetric rooms with reflective walls.

V. Conclusion and Future Work

This paper reviewed the complex image method which models finite-impedance spherical wave scattering in shoebox rooms. A Python implementation and pseudocode was also provided. The advantage of CIM over IM is that it does not make the rigid wall assumption, and can thus model scattering. This has been shown to reduce sweeping echoes that are otherwise observed in IM simulations.

The implementation of CIM is in the frequency domain, so to get a room impulse response, the pressure field at a large number of wave numbers ($> 2 \times T_{60}$) need to be evaluated before computing its inverse Fourier Transform. The computation in the frequency domain involves complex numbers which also increases the complexity. The method is computationally expensive, and takes much longer than Pyroomacoustics. A faster C++ implementation and modeling edge-effects in non-rectangular rooms remain open for future work. Similarly, rigorous comparisons with a wave-based method like BEM is also required.

References

[1] Lauri Savioja and U Peter Svensson, "Overview of geometrical room acoustic modeling techniques," *The Journal of the Acoustical Society of America*, vol. 138, no. 2, pp. 708–730, 2015.

[2] Xiangyang Zeng, Claus Lynge Christensen, and Jens Holger Rindel, "Practical methods to define scattering coefficients in a room acoustics computer model," *Applied acoustics*, vol. 67, no. 8, pp. 771–786, 2006.

[3] Paul T. Calamia and Peter Svensson, "Fast time-domain edge-diffraction calculations for interactive acoustic simulations," *EURASIP Journal on Advances in Signal Processing*, vol. 2007, no. 1, Dec. 2006.

[4] Brian Hamilton and Stefan Bilbao, "FDTD methods for 3-D room acoustics simulation with high-order accuracy in space and time," *IEEE/ACM Transactions on Audio, Speech, and Language Processing*, vol. 25, no. 11, pp. 2112–2124, 2017.

[5] Stephen Kirkup, "The boundary element method in acoustics: A survey," *Applied Sciences*, vol. 9, no. 8, pp. 1642, 2019.

[6] Jont B Allen and David A Berkley, "Image method for efficiently simulating small-room acoustics," *The Journal of the Acoustical Society of America*, vol. 65, no. 4, pp. 943–950, 1979.

[7] Robin Scheibler, Eric Bezzam, and Ivan Dokmanić, "Pyroomacoustics: A python package for audio room simulation and array processing algorithms," in *International Conference on Acoustics, Speech and Signal Processing (ICASSP)*. IEEE, 2018, pp. 351–355.

[8] Enzo De Sena, Niccolo Antonello, Marc Moonen, and Toon Van Waterschoot, "On the modeling of rectangular geometries in room acoustic simulations," *IEEE/ACM Transactions on Audio, Speech, and Language Processing*, vol. 23, no. 4, pp. 774–786, 2015.

[9] Uno Ingard, "On the reflection of a spherical sound wave from an infinite plane," *The Journal of the Acoustical Society of America*, vol. 23, no. 3, pp. 329–335, 1951.

[10] Isadore Rudnick, "The propagation of an acoustic wave along a boundary," *The Journal of the Acoustical Society of America*, vol. 19, no. 2, pp. 348–356, 1947.

[11] Gunnar Taraldsen, "The complex image method," *Wave Motion*, vol. 43, no. 1, pp. 91–97, 2005.

[12] YL Li and Michael J White, "Near-field computation for sound propagation above ground—using complex image theory," *The Journal of the Acoustical Society of America*, vol. 99, no. 2, pp. 755–760, 1996.

[13] Yiu Wai Lam, "Issues for computer modelling of room acoustics in non-concert hall settings," *Acoustical science and technology*, vol. 26, no. 2, pp. 145–155, 2005.
[14] Hermann Weyl, "Ausbreitung elektromagnetischer wellen über einem ebenen leiter," *Annalen der Physik*, vol. 365, no. 21, pp. 481–500, 1919.
[15] Heinrich Kuttruff and Eckard Mommertz, "Room acoustics," in *Handbook of engineering acoustics*, pp. 239–267. Springer, 2012.